Editors' Suggestion | Featured in Physics

Coexistence of Surface Ferromagnetism and a Gapless Topological State in $MnBi_2Te_4$

D. Nevola,[1,*] H. X. Li,[2] J.-Q. Yan,[2] R. G. Moore,[2] H.-N. Lee,[2] H. Miao,[2,†] and P. D. Johnson[1,‡]
[1]Condensed Matter Physics and Materials Science Department, Brookhaven National Laboratory, Upton, New York 11973, USA
[2]Materials Science and Technology Division, Oak Ridge National Laboratory, Oak Ridge, Tennessee 37831, USA

(Received 14 April 2020; revised 30 June 2020; accepted 29 July 2020; published 9 September 2020)

Surface magnetism and its correlation with the electronic structure are critical to understanding the topological surface state in the intrinsic magnetic topological insulator $MnBi_2Te_4$. Here, using static and time resolved angle-resolved photoemission spectroscopy (ARPES), we find a significant ARPES intensity change together with a gap opening on a Rashba-like conduction band. Comparison with a model simulation strongly indicates that the surface magnetism on cleaved $MnBi_2Te_4$ is the same as its bulk state. The inability of surface ferromagnetism to open a gap in the topological surface state uncovers the novel complexity of $MnBi_2Te_4$ that may be responsible for the low quantum anomalous Hall temperature of exfoliated $MnBi_2Te_4$.

DOI: 10.1103/PhysRevLett.125.117205

The combination of magnetism and nontrivial topology opens new routes to realizing novel quantum phenomena such as the quantum anomalous Hall effect (QAHE) and axion electrodynamics [1–12]. The discovery of quantized Hall resistivity in $Cr_{0.15}(Bi_{0.1}Sb_{0.9})_{1.85}Te_3$ demonstrated the first realization of the QAHE without Landau levels [3]. However, the temperature at which the QAHE has been observed is below 100 mK, two orders of magnitude lower than the ferromagnetic ordering temperature, which could be due to large real space electronic inhomogeneities [8,13]. The desire to achieve a higher QAHE temperature has thus motivated the search for intrinsic magnetic topological insulators (TIs).

The *A*-type antiferromagnetic (AFM) $MnBi_2Te_4$ was recently proposed as the first intrinsic magnetic TI [9,11,14–22]. Its crystal structure is shown in Fig. 1(a), where each septuple layer (SL) consists of alternating Bi and Te layers, similar to that in Bi_2Te_3, but with an additional Mn-Te bilayer in the middle. Magnetism originates from the Mn atoms that ferromagnetically order in the *ab* plane and antiferromagnetically order along the [0001] direction [15,23]. The topological surface state (TSS) arises from the band inversion between the Bi and Te p_z bands at the Γ point. Below $T_N \sim 25$ K the *A*-type AFM is expected to open a gap in the massless Dirac cone on the (0001) surface [Figs. 1(b) and 1(c)]. This gap opening is thought to induce QAHE or axion states, which form depending on the number of SLs [10,11,17]. More recently, the quantized Hall resistivity has been observed in exfoliated $MnBi_2Te_4$ [24,25]. While the original angle-resolved photoemission spectroscopy (ARPES) study of $MnBi_2Te_4$ single crystals supports a gapped TSS below T_N [15], more recent ARPES studies show that the dispersion of the TSS remains unchanged below and above T_N with no gap forming [9,16,17,19,20,26]. A key step to resolving this controversy is to understand whether or not the surface is magnetically ordered below the bulk T_N [9,16,17,19,20,26]. Here, we use static and time resolved ARPES (TRARPES) with full polarization control to prove that the magnetic order is retained at the surface, but fails to induce a gap in the TSS. Our results uncover a novel complexity of the intrinsic magnetic TI that may be responsible for the low QAHE temperature of 1.5 K in $MnBi_2Te_4$ [24,25].

The laser-based ARPES was performed at Brookhaven National Laboratory using an SES-2002 analyzer. The

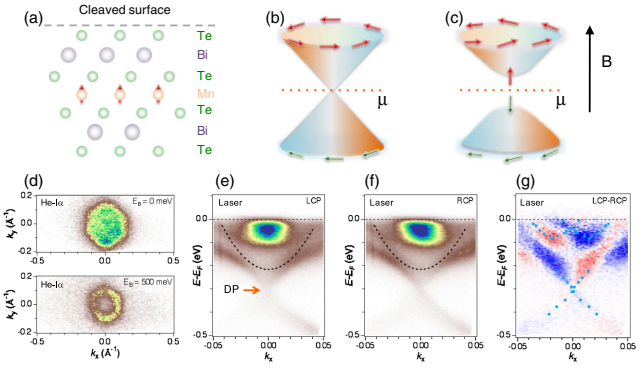

FIG. 1. Crystal and band structure of the intrinsic magnetic TI $MnBi_2Te_4$. (a) The SL of $MnBi_2Te_4$. Schematic plots of the topological surface state without (b) and with (c) effective ferromagnetic field. (d) ARPES constant energy plot taken with He-Iα = 21.2 eV at E_F and $E_B = 0.5$ eV. (e) and (f) are ARPES intensity plots measured with LCP and RCP across the Γ point, taken in the paramagnetic state at 40 K. The red arrow in (e) indicates the Dirac point at $E_B = 0.3$ eV. The black curve shows the approximate position of the bulk conduction band. (g) shows the intensity difference between LCP and RCP. The cyan markers indicate the Rashba-like conduction band and massless Dirac cone.

He-Iα measurement was performed at Oak Ridge National Laboratory using a DA30 analyzer. The samples were cleaved *in situ*, and experiments were performed at a base pressure of 4×10^{-11} torr. For the laser-based source, we used the fourth harmonic of a 800 nm beam operating at 250 kHz. The output of a Ti:sapphire oscillator (Coherent Inc. Vitara T) was used to seed a regenerative amplifier (Coherent Inc. RegA 9050) in order to produce pulses of 30 nm bandwidth and 70 fs. Fourth harmonic generation was then achieved through a series of nonlinear processes using β-BaB_2O_4 crystals. The fourth harmonic was subsequently compressed using a prism compressor. For the TRARPES measurements, the 800 nm fundamental pulses were used to pump the sample and a delay stage was used to control the delay time in between the two pulses. The Fermi level location was calibrated using photoemission from polycrystalline gold. The pump-probe temporal overlap and resolution was determined through measurements at high energies in Bi_2Se_3. For the laser-based ARPES measurements, the resolution was 29 meV, and for the TRARPES measurements, the energy and time resolutions were 50 meV and 180 fs, respectively.

The band structure of $MnBi_2Te_4$ consists of several bands within a few hundred meV of E_F. Figures 1(d)–1(f) show the normal state spectral function near the Γ point, placing the Dirac point (DP) approximately 300 meV below E_F with a dispersive bulk conduction band 80 meV above the DP. In addition, a feature with large intensity within 100 meV of E_F has been observed at the zone center [16,20]. This feature is also clear in the constant energy maps taken with He-Iα, where we observe a hexagonal surface without states at the zone center 200 meV below the DP, and a hexagonal surface with states at the zone center at E_F [Fig. 1(d)]. Since the intensity of this feature is known to be enhanced at low photon energies [16,20], we use laser-based photoemission to probe its properties and temperature dependence.

We first examine the circular dichroism (CD) of these bands above T_N. Figure 1(g) shows the spectral difference between the left (LCP) and right (RCP) circularly polarized light, where we observe a rich dichroic dependence. Such dichroism is known to be indirect evidence of spin separation [27]. Here we focus on the Dirac cone and the high intensity feature near E_F. First, each half of the Dirac cone shows the opposite chiral dependence, expected for a topological surface state. This result agrees with direct spin-dependent measurements using spin ARPES [22]. Second and most importantly, we find that the high intensity feature near E_F consists of two parabolic bands that are separated in $\mathbf{k}$ with clear CD, reminiscent of a Rashba state [27–29]. Notably, the left-right intensity asymmetry of these two bands are opposite to each other, supporting the presence of strong spin-orbit coupling [27–29]. While these Rashba-like bands have been inferred in previous studies [20,26], our CD study firmly establishes its band dispersion with strong evidence of spin-momentum locking,

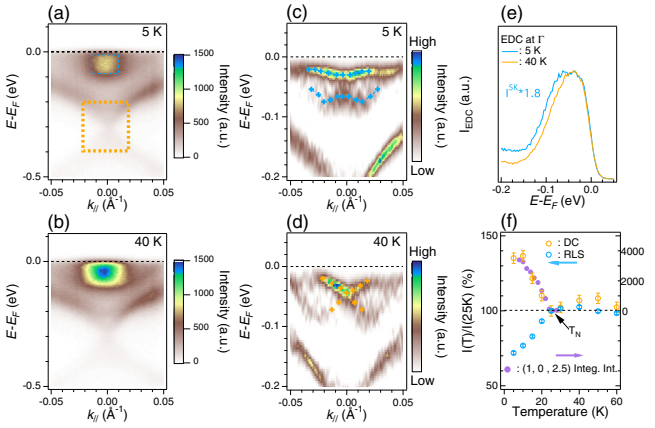

FIG. 2. Evidence of surface magnetic order below T_N. (a) and (b) are ARPES intensity plots at 5 and 40 K, respectively. These plots are obtained by adding LCP and RCP to reduce the polarization matrix elements effects. (c) and (d) are the curvature plots of (a) and (b) respectively in a narrower energy range. Cyan and orange curves act as guide to the eye indicating the Rashba-like band at 5 and 40 K. Because of the presence of the bulk state, the Rashba-like splitting derived from the curvature analysis is slightly larger than that shown in Fig. 1(g). A direct comparison of EDCs below (5 K) and above (40 K) T_N at the Γ point is shown in (e). (f) shows the temperature-dependent intensity change of the Rashba-like band (cyan) and the TSS (orange). The integration areas are shown in (a). Purple circles are the integrated intensity of magnetic Bragg peak at $\boldsymbol{Q} = (1, 0, 2.5)$ [23].

as expected for a Rashba state. Since $MnBi_2Te_4$ preserves the inversion symmetry in its bulk electronic and crystal structure [9,11,18], the Rashba-like state at the Γ point with clear CD must be a surface effect. Indeed, the intensity of the Rashba-like state shows a similar photon-energy dependence to the TSS, with both showing strong emission near 7 eV and significant suppression above 10 eV [16,17,20].

We now turn to explore the temperature dependence of the Rashba-like state and TSS. Figures 2(a) and 2(b) show the raw data acquired as the sum of LCP and RCP below and above the magnetic ordering temperature, respectively. Before moving to discuss the Rashba-like state, we note that in agreement with more recent ARPES studies [9,16,17,19,20,26], the dispersion of the gapless TSS, within our experimental resolution, remains unchanged above and below the bulk T_N [30]. The Rashba-like state, however, shows some subtle differences. Applying the curvature analysis [33] above the magnetic ordering temperature [Fig. 2(d)] confirms the Rashba-like splitting shown in Fig. 1(g). The observed momentum and energy splittings are approximately 0.025 Å^{-1} and 50 meV, respectively. Applying the curvature analysis shows, in agreement with a recent report [34], a band gap of about 35 meV at the Kramers point below magnetic ordering [Fig. 2(c)]. More concrete evidence of the changes to the Rashba-like bands with magnetic ordering can be extracted directly from the raw data by taking energy distribution

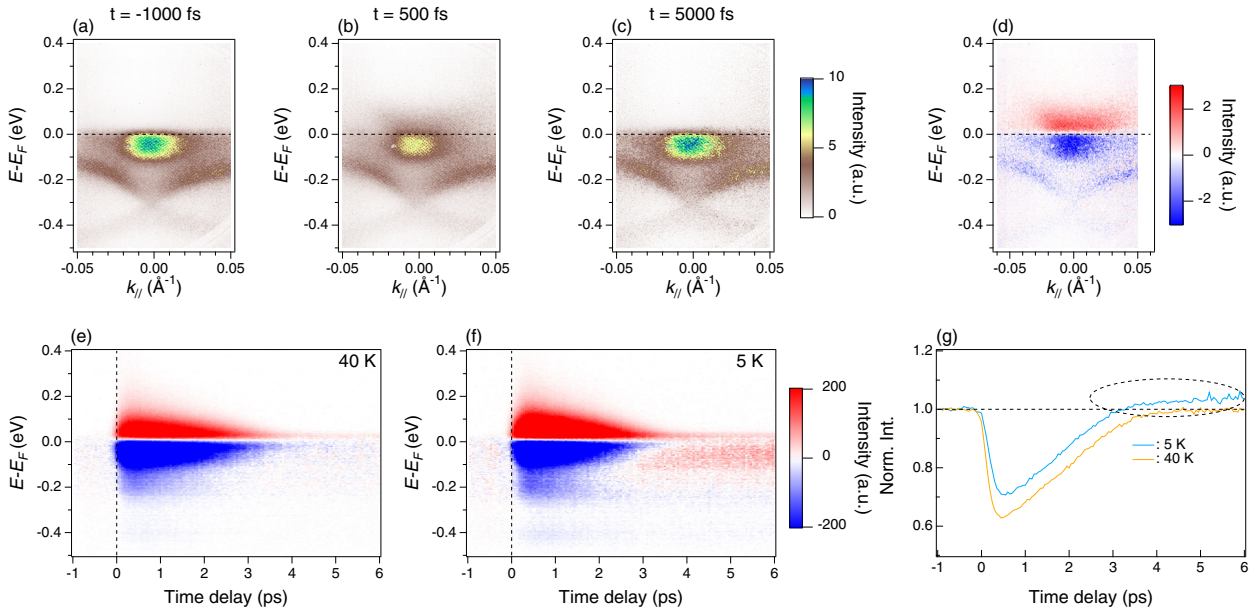

FIG. 3. Intensity anomaly revealed by TRARPES. (a)–(c) TRARPES intensity plots with different time delays. The spectra were collected at 5 K. (d) shows the representative intensity difference between (a) and (b). (e) and (f) are the k-integrated spectra as a function of delay time taken at 40 and 5 K, respectively. (g) Integrated intensity of the Rashba-like state as a function of time delay. Cyan and orange curves represent 5 and 40 K, respectively. The dashed oval highlights the intensity increase after 4 ps.

curves (EDCs) through the Γ point [Fig. 2(e)]. We immediately see a qualitative difference in that the band becomes broader at the low temperature, opposite to that expected with typical temperature broadening. Additionally the EDC peak maximum flattens, offering further supporting evidence that the Kramers point splits into two bands [30].

In addition to the gap opening, we observe significant intensity changes to both the Rashba-like state and TSS below and above T_N, as is immediately noticeable in the intensity plots [Figs. 2(a) and 2(b)]. To quantify this effect, we plot the integrated intensities in the dashed rectangular areas shown in Fig. 2(b) as a function of temperature [Fig. 2(f)]. We see that the magnetic ordering has opposite effects on the Dirac cone and the Rashba-like state. The intensity change agrees with the temperature-dependent bulk magnetic order-parameter determined by neutron scattering [18]. Since both of these states are of surface origin, Fig. 2(f) provides strong evidence that the surface electronic states "feel" the bulk magnetic ordering.

To further demonstrate the spectral weight change, we perform TRARPES both above and below T_N. A summary of our findings is shown in Figs. 3(e)–3(g), where we display the k-integrated spectra as a function of delay time. In Figs. 3(a)–3(c), we show the ARPES intensity plots at different time delays. Figure 3(d) shows a representative intensity difference between 500 fs and −1000 fs. Red and blue colors represent intensity increase and decrease, respectively, with respect to the spectrum prior to the introduction of the pump pulse. When the system is pumped at an initial temperature of 40 K [Fig. 3(e)], we clearly see that the system relaxes back to its initial value after a delay time of approximately 4 ps, albeit at a slightly higher temperature (the higher temperature can be seen by noting the slight positive signal just above and the slight negative signal just below E_F). This can be understood qualitatively by the two-temperature model, whereby the pump pulse induces a rapid increase in the electronic temperature that ultimately equilibrates with the lattice temperature through electron-phonon scattering, resulting in a steady state equal to that prior to the pump, but at a slightly higher temperature [35,36]. In Fig. 3(f), we show the same data as Fig. 3(e), but pumped while the system is magnetically ordered. At long delays above 4 ps, we observe the same intensity feature as seen in the data above T_N along with an additional intensity increase within 150 meV of E_F, corresponding to the location of the Rashba-like state. In order to track this more clearly, we integrate over the Rashba-like state and display the resulting intensity as a function of delay time [Fig. 3(g)]. We can see that the intensity of the band increases by approximately 3% compared to its negative time value. This observation qualitatively agrees with Fig. 2(f), where we showed the equilibrium changes to the spectral weight as a function of temperature. The 3% change in the Rashba-like state signifies a temperature increase of only a few degrees when compared with Fig. 2(e). Thus, two different experiments show the same spectral weight change in the ARPES spectra with magnetic ordering.

Both the ARPES intensity changes and the gap opening on the Rashba-like state strongly indicate that the surface of

cleaved $MnBi_2Te_4$ is magnetically ordered. This conclusion is consistent with magnetic susceptibility measurements of exfoliated $MnBi_2Te_4$ [17,24,25] and a magnetic force microscopy study of cleaved bulk $MnBi_2Te_4$ [37]. Recently, it has been speculated that the top SL may favor a different type of magnetic ordering, such as G-type antiferromagnetic order [26] or ferromagnetic (FM) order with spin orientation different from that in the bulk [20]. To check these possibilities, we simulate our 40 K data with a simple Rashba Hamiltonian using our extracted parameters and explore the effects of different magnetically ordered configurations. At 40 K, the effective Hamiltonian can be written as

$$H_R(\mathbf{k}) = \left(\frac{\hbar^2 k^2}{2m^*} - \mu\right)\mathbf{I}_{2\times 2} + v_F(k_y\sigma_x - k_x\sigma_y) = \begin{pmatrix} \frac{\hbar^2 k^2}{2m^*} - \mu & v_F(k_x + ik_y) \\ v_F(k_x - ik_y) & \frac{\hbar^2 k^2}{2m^*} - \mu \end{pmatrix}, \quad (1)$$

where $\mathbf{I}_{2\times 2}$ and σ_i $(i = x, y, z)$ are the 2-by-2 unit matrix and the Pauli matrices, respectively. The eigenvalues of Eq. (1) are $E(\mathbf{k})_\pm = (\hbar^2 k^2/2m^*) - \mu \pm v_F|\mathbf{k}|$. Figure 4 shows the simulated single-particle spectral function:

$$A(\mathbf{k}, \omega) = \frac{1}{\pi}\frac{\Gamma}{\{[\omega - E(\mathbf{k})]^2 + \Gamma^2\}}, \quad (2)$$

where $\Gamma = 0.04$ eV is the quasiparticle lifetime. $E(\mathbf{k})$ is determined by fitting of the extracted Rashba-like band dispersion. In the G-type AFM phase, the surface unit cell is doubled, however the Rashba band remains gapless [20,26]. Therefore, the observation of the gapped Rashba-like band below T_N excludes the surface AFM order. For the FM order, the effective Hamiltonian can be written as

$$H_{\mathrm{FM}}(\mathbf{k}) = H_R(\mathbf{k}) + \sum_i \Delta_i\sigma_i. \quad (3)$$

The eigenvalues of Eq. (3) are $E(\mathbf{k})_\pm = (\hbar^2 k^2/2m^*) - \mu \pm \sqrt{\Delta_z^2 + (v_F k_x + \Delta_x)^2 + (v_F k_y - \Delta_y)^2}$. Figures 4(b) and 4(c) show the simulated $A(\mathbf{k}, \omega)$ with $\mathbf{\Delta} = (0, 0, \Delta_z)$ and $(\Delta_x, 0, 0)$, respectively. It is clear that the out-of-plane spin orientation best describes our data, while the in-plane spin orientation shifts the two Rashba bands in opposite energy directions, inconsistent with our observations. Interestingly, the simulation also shows a 30% intensity drop of the Rashba band, again consistent with our experimental observation.

The gapped Rashba-like state and the dramatic intensity change below T_N have important implications for the topological states in $MnBi_2Te_4$. First principles calculations show that, in the presence of surface ferromagnetism, the gap in the TSS is about 60 meV [20]; the same magnitude as the observed gap on the Rashba-like state.

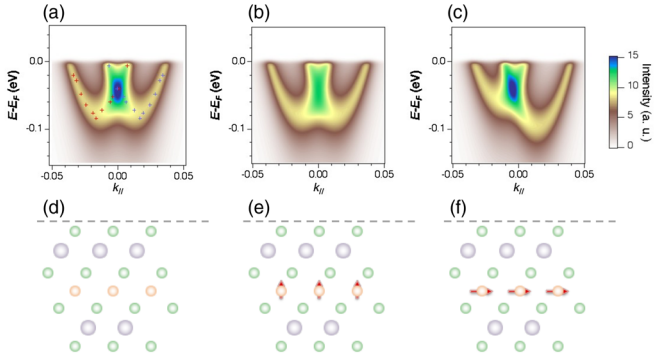

FIG. 4. (a)–(c) show simulated single-particle spectral functions for (d) nonmagnetic SL, (e) FM SL with out-of-plane spin orientation, and (f) FM SL with in-plane spin orientation, respectively.

The absence of change in the TSS dispersion within our experimental resolution proves that the effect of surface ferromagnetism on the TSS is extremely small. To reconcile this discrepancy, we note that the wave function of the TSS will take the form $\phi_0(z)u(\mathbf{k}_{||})e^{-i\mathbf{r}_{||}\cdot\mathbf{k}_{||}}$, where $\phi_0(z) \propto e^{-z/l_z}$, corresponds to the exponentially decaying component in the z direction with decay length l_z. We suggest that l_z is longer than the calculations suggest. Indeed, the dramatic intensity change below T_N on the fully occupied DP [Fig. 2(f)] suggests that l_z is larger than the photoelectron penetration depth, l_{phe}, at 6.2 eV, which is greater than 20 Å. Similarly the suppressed intensity of the TSS above 10 eV [16,17,20] also supports our scenario as the shorter l_{phe} is expected to have smaller surface state cross-sections. We thus call for comprehensive theoretical studies of the surface wave function localization and its relation to magnetic order.

Another implication of our study is that the insulating behavior of exfoliated even layer $MnBi_2Te_4$ may simply arise from the coupling between the top and bottom layers [2] and the quantum Hall effect (QHE) is only realized under an external magnetic field that is larger than the spin-flop field [24]. We note that in odd layered $MnBi_2Te_4$, the QAHE is observed at a condition where the spin-flop transition is completely suppressed [25]. We thus speculate that, in such a case, spins between adjacent SL are pinned and ferromagnetically ordered. Indeed, the QAHE temperature in odd layered $MnBi_2Te_4$ is close to the QHE temperature in even layered $MnBi_2Te_4$ above the spin-flop transition [24].

In summary, by analyzing the temperature and time-dependent ARPES spectra, we find a strong FM effect on surface-related electronic states. Our results uncover a novel complexity of the intrinsic magnetic TI that may be responsible for the low QAHE temperature in $MnBi_2Te_4$.

H. M. acknowledges M. H. Du, H. X. Fu, S. Okamoto, B. H. Yan, and T. T. Zhang for insightful discussions. Work at Brookhaven National Laboratory was supported by the

U.S. Department of Energy, Office of Science, Office of Basic Energy Sciences, under Contract No. DE-SC0012704 (Laser-ARPES and data interpretation). Work at Oak Ridge National Laboratory (ORNL) was supported by the U.S. Department of Energy, Office of Science, Basic Energy Sciences, Materials Sciences and Engineering Division (sample synthesis and ARPES). H. M. and R. G. M. were supported by the Laboratory Directed Research and Development Program of Oak Ridge National Laboratory, managed by UT-Battelle, LLC, for the U. S. Department of Energy (ARPES and data interpretation).

*nevola@bnl.gov
†miaoh@ornl.gov
‡pdj@bnl.gov

[1] R. Li, J. Wang, X.-L. Qi, and S.-C. Zhang, Nat. Phys. **6**, 284 (2010).
[2] R. Yu, W. Zhang, H.-J. Zhang, S.-C. Zhang, X. Dai, and Z. Fang, Science **329**, 61 (2010).
[3] C.-Z. Chang *et al.*, Science **340**, 167 (2013).
[4] J. G. Checkelsky, R. Yoshimi, A. Tsukazaki, K. S. Takahashi, Y. Kozuka, J. Falson, M. Kawasaki, and Y. Tokura, Nat. Phys. **10**, 731 (2014).
[5] J. Wang, B. Lian, X.-L. Qi, and S.-C. Zhang, Phys. Rev. B **92**, 081107(R) (2015).
[6] T. Morimoto, A. Furusaki, and N. Nagaosa, Phys. Rev. B **92**, 085113 (2015).
[7] M. Mogi, M. Kawamura, A. Tsukazaki, R. Yoshimi, K. S. Takahashi, M. Kawasaki, and Y. Tokura, Sci. Adv. **3**, eaao1669 (2017).
[8] Y. Tokura, K. Yasuda, and A. Tsukazaki, Nat. Rev. Phys. **1**, 126 (2019).
[9] J. Li, Y. Li, S. Du, Z. Wang, B.-L. Gu, S.-C. Zhang, K. He, W. Duan, and Y. Xu, Sci. Adv. **5**, eaaw5685 (2019).
[10] Y. Xu, Z. Song, Z. Wang, H. Weng, and X. Dai, Phys. Rev. Lett. **122**, 256402 (2019).
[11] D. Zhang, M. Shi, T. Zhu, D. Xing, H. Zhang, and J. Wang, Phys. Rev. Lett. **122**, 206401 (2019).
[12] S. Nie, Y. Sun, F. B. Prinz, Z. Wang, H. Weng, Z. Fang, and X. Dai, Phys. Rev. Lett. **124**, 076403 (2020).
[13] I. Lee, C. K. Kim, J. Lee, S. J. L. Billinge, R. Zhong, J. A. Schneeloch, T. Liu, T. Valla, J. M. Tranquada, G. Gu, and J. C. S. Davis, Proc. Natl. Acad. Sci. U.S.A. **112**, 1316 (2015).
[14] Y. Gong *et al.*, Chin. Phys. Lett. **36**, 076801 (2019).
[15] M. M. Otrokov *et al.*, Nature (London) **576**, 416 (2019).
[16] Y. J. Chen, L. X. Xu, J. H. Li, Y. W. Li, H. Y. Wang, C. F. Zhang, H. Li, Y. Wu, A. J. Liang, C. Chen, S. W. Jung, C. Cacho, Y. H. Mao, S. Liu, M. X. Wang, Y. F. Guo, Y. Xu, Z. K. Liu, L. X. Yang, and Y. L. Chen, Phys. Rev. X **9**, 041040 (2019).
[17] B. Chen *et al.*, Nat. Commun. **10**, 4469 (2019).
[18] J.-Q. Yan, S. Okamoto, M. A. McGuire, A. F. May, R. J. McQueeney, and B. C. Sales, Phys. Rev. B **100**, 104409 (2019).
[19] H. Li *et al.*, Phys. Rev. X **9**, 041039 (2019).
[20] Y.-J. Hao *et al.*, Phys. Rev. X **9**, 041038 (2019).
[21] E. D. L. Rienks *et al.*, Nature (London) **576**, 423 (2019).
[22] R. C. Vidal *et al.*, Phys. Rev. B **100**, 121104(R) (2019).
[23] J.-Q. Yan, Q. Zhang, T. Heitmann, Z. Huang, K. Y. Chen, J.-G. Cheng, W. Wu, D. Vaknin, B. C. Sales, and R. J. McQueeney, Phys. Rev. Mater. **3**, 064202 (2019).
[24] C. Liu, Y. Wang, H. Li, Y. Wu, Y. Li, J. Li, K. He, Y. Xu, J. Zhang, and Y. Wang, Nat. Mater. **19**, 522 (2020).
[25] Y. Deng, Y. Yu, M. Z. Shi, Z. Guo, Z. Xu, J. Wang, X. H. Chen, and Y. Zhang, Science **367**, 895 (2020).
[26] P. Swatek, Y. Wu, L.-L. Wang, K. Lee, B. Schrunk, J. Yan, and A. Kaminski, Phys. Rev. B **101**, 161109(R) (2020).
[27] Y. Wang and N. Gedik, Phys. Status Solidi RRL **7**, 64 (2013).
[28] G. Bian, L. Zhang, Y. Liu, T. Miller, and T.-C. Chiang, Phys. Rev. Lett. **108**, 186403 (2012).
[29] H. Bentmann, H. Maaß, E. E. Krasovskii, T. R. F. Peixoto, C. Seibel, M. Leandersson, T. Balasubramanian, and F. Reinert, Phys. Rev. Lett. **119**, 106401 (2017).
[30] See Supplemental Material at http://link.aps.org/supplemental/10.1103/PhysRevLett.125.117205 for more detailed data and analysis including Lucy-Richardson deconvolution, a full temperature dependence and a description of the gapless surface state, which includes Refs. [31,32].
[31] J. D. Rameau, H.-B. Yang, and P. D. Johnson, J. Electron Spectrosc. Relat. Phenom. **181**, 35 (2010).
[32] I. I. Klimovskikh, A. M. Shikin, M. M. Otrokov, A. Ernst, I. P. Rusinov, O. E. Tereshchenko, V. A. Golyashov, J. Snchez-Barriga, A. Y. Varykhalov, O. Rader, K. A. Kokh, and E. V. Chulkov, Sci. Rep. **7**, 3353 (2017).
[33] P. Zhang, P. Richard, T. Qian, Y.-M. Xu, X. Dai, and H. Ding, Rev. Sci. Instrum. **82**, 043712 (2011).
[34] D. A. Estyunin, I. I. Klimovskikh, A. M. Shikin, E. F. Schwier, M. M. Otrokov, A. Kimura, S. Kumar, S. O. Filnov, Z. S. Aliev, M. B. Babanly, and E. V. Chulkov, APL Mater. **8**, 021105 (2020).
[35] P. B. Allen, Phys. Rev. Lett. **59**, 1460 (1987).
[36] L. Rettig, R. Cortés, H. S. Jeevan, P. Gegenwart, T. Wolf, J. Fink, and U. Bovensiepen, New J. Phys. **15**, 083023 (2013).
[37] P. M. Sass, J. Kim, D. Vanderbilt, J. Yan, W. Wu, Phys. Rev. Lett. **125**, 037201 (2020).